Proceedings World Geothermal Congress 2023
Beijing, China, April 17 – 21, 2023

Geochemical characterization and resource assessment of a low to medium temperature hydrothermal system within the Sabinas basin, Coahuila, Mexico.

Sergio Villeda[1], Edgar R. Santoyo[1], Mirna Guevara[1], Eduardo González-Partida[2], Enrique Portugal[3]

1 Instituto de Energías Renovables, UNAM. Xochicalco s/n Temixco 62580, México. 2 Centro de Geociencias. UNAM Campus Juriquilla Blvd. Juriquilla 3001. Querétaro 76230. México. 3 Gerencia de Geotermia, Instituto Nacional de Electricidad y Energías Limpias, Reforma 113 Col. Palmira, Cuernavaca, Morelos, 62490, Mexico

seviv@ier.unam.mx; esg@ier.unam.mx

Keywords: Sedimentary basin, Deep aquifer, geothermal resource

ABSTRACT

The Northeast of Mexico is known for the exploitation of hydrocarbons, moreover, the region also contains thermal manifestations that have not been studied in detail to determine their characteristics and to evaluate their possible use in the generation of electricity, and/or in direct uses. This work presents a preliminary geothermal prospecting study of thermal manifestations in the Escobedo area, Coahuila, within the Sabinas basin. The work considered a review and compilation of information from the area, including information from gas wells, as well as a first campaign to collect samples from different water bodies, including hot springs, rivers, and water wells, to the characterization of major elements and stable isotopes. This geochemical information was used to classify the fluids and determine their origin and likely producing reservoir temperatures. Preliminary results indicate the presence of two types of waters: thermal Ca2-SO4 waters and cold Ca2-HCO3 waters, which seem to indicate a meteoric origin and whose recharge occurs at altitudes like those of the mountains that delimit the study area, discharging from fractures in the base of anticlines. Geothermometric temperatures estimated in hot waters (discharged from thermal springs and gas well) indicate a low to medium temperature system, with equilibrium values of the order of 87.0 ± 17°C, consistent with those predicted by a silica-enthalpy mixing model. The probable reservoir would be in the La Virgen formation, according to available gas well information. The results and analysis of information led to the proposal of a conceptual model of the system, which is the base for the resource assessment through the volumetric method and Monte Carlo simulations. These results allow the knowledge of the geothermal resources in the Sabinas basin and the possible synergies between the oil industry (Infrastructure and related studies) and the development of geothermal energy in Mexico.

1. INTRODUCTION

Sedimentary basins are known for the coexistence of non-renewable resources such as oil and gas and for hosting geothermal systems, such as hydrothermal or geopressured, either for electricity generation or direct use. This coexistence between hydrocarbons and geothermal systems presents advantages for the development of geothermal energy, since the studies, as well as the infrastructure already developed by the hydrocarbon industry, can reduce costs when exploring and exploiting a geothermal resource within these basins (Tester et al., 2015).

Mexico has some sedimentary basins in which the Sabinas basin stands out, known for the exploitation of natural gas (Eguiluz de Antuñano, 2001). This basin presents various hydrothermal manifestations that have not been studied in detail. As this basin has been studied for the exploitation of hydrocarbons, it is important to take advantage of the existing information to elevate the understanding of geothermal systems within these geologic settings.

Thus, in this work, the hydrothermal manifestations of the Escobedo area, Coahuila, within the Sabinas basin are studied, applying geochemical and geothermometric analysis, using information from gas wells drilled within the zone, as well as from various studies in the area, offering relevant information for the understanding of the geothermal resources within this basin, its potential, as well as to offer information that could contribute to the subsequent phases of use of these resources.

2. GEOLOGICAL FRAMEWORK

The study zone is located in northeast Mexico, within the Sabinas basin. This basin was formed during the Jurassic and Triassic, when the rift that separated North American and South American plates (Padilla Y Sanchez, 1986) created grabens and blocks that permitted the deposition of sediments, pilling up a column of more than 5000 meters (Cuevas Leree 1984; Eguiluz de Antuñano 2001). When the stage of breaking and rift stopped, the basin experienced continuous subsidence until the beginning of the Paleogene, when the Laramide orogeny compressed and fractured the pile of sediments, leading to the formations of high relieve anticlines and wide valley synclines (Cuevas Leree, 1984; Molina et al., 2004).

The rocks in the lithological column vary from shales, limestone, sandstone, and conglomerate, where the older layers were deposited in different environments (Marine and continental) due to different stages of sea transgressions (Corona-Esquivel et al., 2006). Finally, during the orogeny, the compression forces created fractures and structures useful for the movement of fluids, in the case of water, domaining the hydrology (Wolaver et al., 2013) while the structural traps permitted the concentration of hydrocarbons (These

traps are the main objective for drilling natural gas wells). At the local scale, the study zone is crossed by two anticlines, separated by a syncline, where most of the springs are located at the base of the anticlines (Fig. 1).

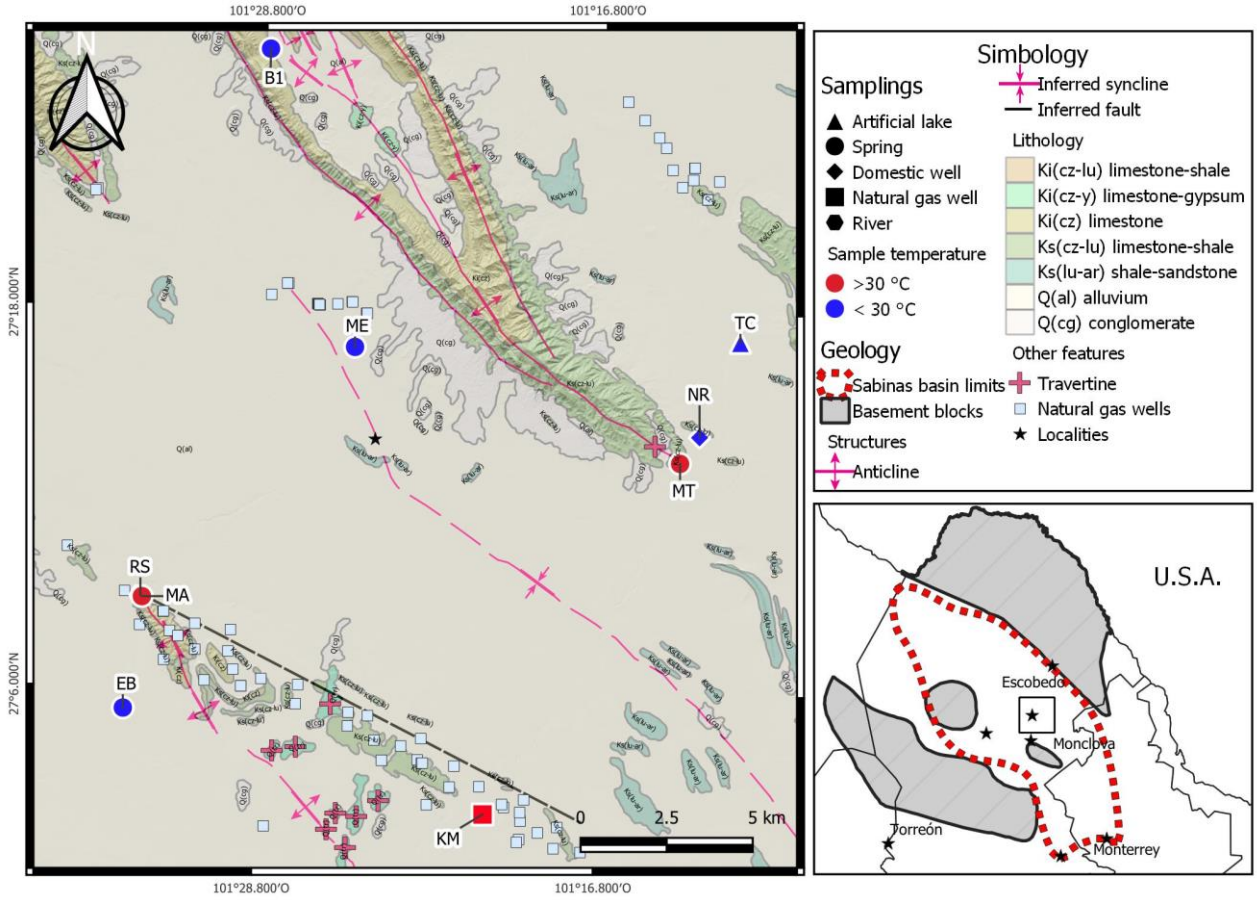

Figure 1: Geologic and regional maps of the study zone. Including sampling sites.

3. DATA AND METHODS

A compilation of previous studies in the area was carried out, including geological and hydrological studies. Also, information from natural gas wells within the area was requested from the Comisión Nacional de Hidrocarburos (CNH). This was to design and determine promising sites for sampling. 10 sites were designed to conduct water samplings: 3 cold springs (B1, EB, ME), two hot springs (MA, MT), one natural gas well with thermal water discharge (KM), one domestic well (NR), water from the main river of the basin (RS) and a superficial body (TC). Samplings were conducted in February 2020.

Water samples for major dissolved ions as well as stable isotopes were filtrated with an 0.45 cellulose acetate membrane and then were collected in 60 ml and 20 ml polyethylene bottles (previously washed with acid and rinsed with deionized water), sealed, and put in refrigeration until their analysis in the laboratory. The samples for the determination of cations were acidified with ultrapure HNO3 until the pH was less than 3. During the samplings, physicochemical parameters (temperature, electrical conductivity, and pH) were measured in situ with a portable multimeter.

The techniques used for the analysis of anions and cations were ion chromatography and inductively coupled plasma atomic emission spectroscopy (ICP-OES) respectively, while the stable isotopes were determined by isotope-ratio mass spectrometry (IR-MS). All analyses were carried out in the geochemistry laboratory of the Instituto Nacional de Electricidad y Energías Limpias (INEEL).

4. RESULTS AND DISCUSSION

The results of the physicochemical parameters and the chemical composition of the waters are shown in table 1. The maximum temperature corresponds to the natural gas well with 65.4 °C and cold samples have temperatures < 30 °C (some springs and surface water bodies). Subsurface waters are characterized by a neutral or slightly acidic pH ranging from 6.73 to 7.018 while surface waters exhibit basic pHs. Electric conductivity (EC) in samples shows a range between 1159 and 6209 $\mu S/cm$, where the lower conductivities correspond to cold springs, intermediate EC to thermal samples, and upper values to surface waters.

The main ions present in the waters are SO4, and HCO3 for anions, and Ca2, Mg2, and Na for cations. An ion imbalance < 10 % in samples was considered an indication of quality, for most of the samples this was achieved, except for NR.

Table 1: Physicochemical parameters and chemical composition for the waters sampled within the study area (Major and other elements in mg/kg and stable isotopes as 0/00 relative to VSMOW)

	B1	EB	KM	MA	ME	MT	NR	RS	TC
Sample type	Spring	Spring	Natural gas well	Spring	Spring	Spring	Domestic well	River water	Artificial lake
Physicochemical parameters									
Temp[1]	26.1 ± 0.1	23.5 ± 0.1	65.4 ± 0.1	30.6 ± 0.2	22.7 ± 0.7	42.4 ± 0.0	19.6 ± 0.1	17.4 ± 0.1	15.2 ± 0.0
pH	7.01 ± 0.01	6.96 ± 0.01	6.73 ± 0.03	6.81 ± 0.07	7.12 ± 0.08	6.98 ± 0.01	7.19 ± 0.16	8.03 ± 0.03	8.13 ± 0.08
EC[2]	1806 ± 3	4388 ± 4	2749 ± 83	3976 ± 11	1166 ± 7	2260 ± 0	2886 ± 7	4260 ± 0	6090 ± 0
Major cations									
Li	< 0.027	0.058	0.033	0.071	0.05	0.029	0.061	0.057	0.212
Na	7.901	338.821	90.305	202.363	44.571	19.269	40.398	310.246	516.351
K	1.155	6.53	2.886	3.869	1.325	2.036	11.507	6.618	7.123
Mg2	57.755	179.755	109.831	146.421	30.121	84.981	124.723	166.842	272.935
Ca2	407.033	513.929	528.192	582.703	201.485	452.595	535.812	484.75	529.94
Major anions									
F	4.57	3.93	8.48	5.88	3.83	7.15	< 0.3	4.11	5.97
Cl	5.28	358	142	367	31.2	29.6	2.46	378	990
SO4	983	2130	1810	1940	314	1390	6.49	1940	2210
Br	< 0.3	1.54	< 0.7	1.48	< 0.3	< 0.7	< 0.7	< 0.7	2.52
HCO3	228.791	339.241	224.846	284.016	390.522	213.012	228.791	331.352	228.791
II[3] (%)*	1.72	-4.19	-7.5	-5.33	1.77	-4.91	81.53	-4.69	-4.28
Stable isotopes									
δ 18O	-6.6	-6.2	-7.3	-6.4	-5.3	-6.7	-6.3	-6.1	-2.4
δ D	-39.2	-44.2	-47.1	-44.1	-36	-42.3	-41.2	-42.9	-23.6
Other elements									
SiO2	11.636	20.795	34.169	26.136	23.821	36.504	21.331	21.331	28.849

1: Surface temperature [°C]. 2: Electric conductivity [$\mu S/cm$].3: Ionic imbalance

4.1 Geochemistry, origin, and ion evolution

Major ion composition was plotted in the piper diagram (Figure 2). Two main groups can be identified, the first one, Ca2-HCO3 waters in two sites (ME, NR), and Ca2-SO4 waters for all thermal samples and the rest of the samples. Additionally, for this last group, an increase in Cl and Na+K is observed, mainly in surface waters. Electric conductivity increase is also shown in the piper plot, where the lower values correspond to the Ca-HCO3 waters, then EC is increased in the second water group, reaching the maximum values in surface waters, where Na and Cl are concentrated.

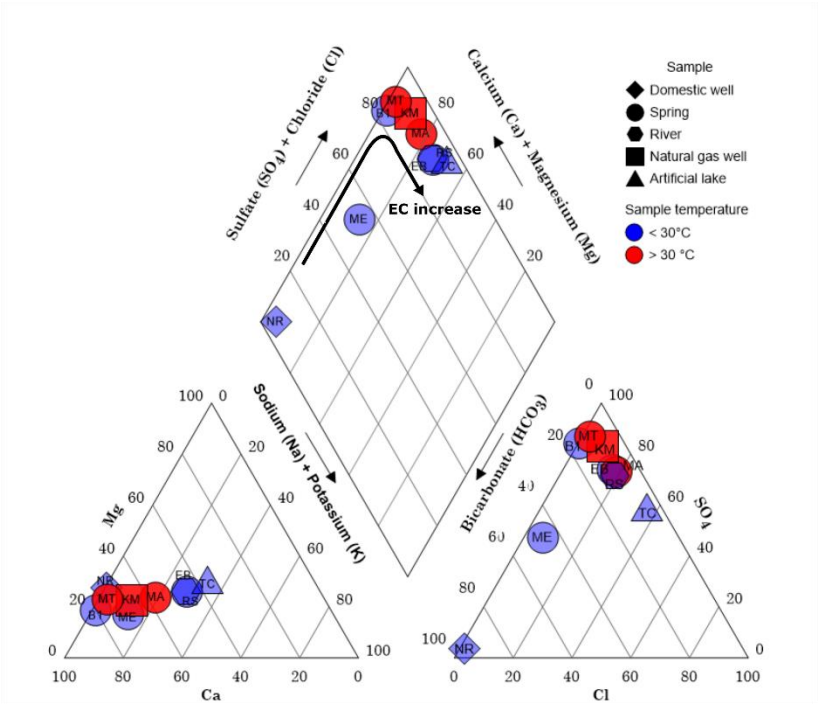

Figure 2:Piper diagram for the classification of the waters, including the increment of electric conductivity (EC) represented by the black arrow

Stable isotope water composition is presented in the δD vs δ 18O plot in figure 3 along with the Global meteoric line (Craig, 1961) and local meteoric line (Cortés et al., 1997). The isotopic signature for the waters in the study zone seems to indicate a meteoric origin, as most of the samples are near and parallel to both meteoric water lines, including one sample with an evaporation firm as it is enriched with 18O. For the other samples, we can observe that the most depleted water (KM) corresponds to the highest temperature, while the most enriched sample (without evaporation) has associated with the lowest EC, between these two samples, the remaining samples are clustered.

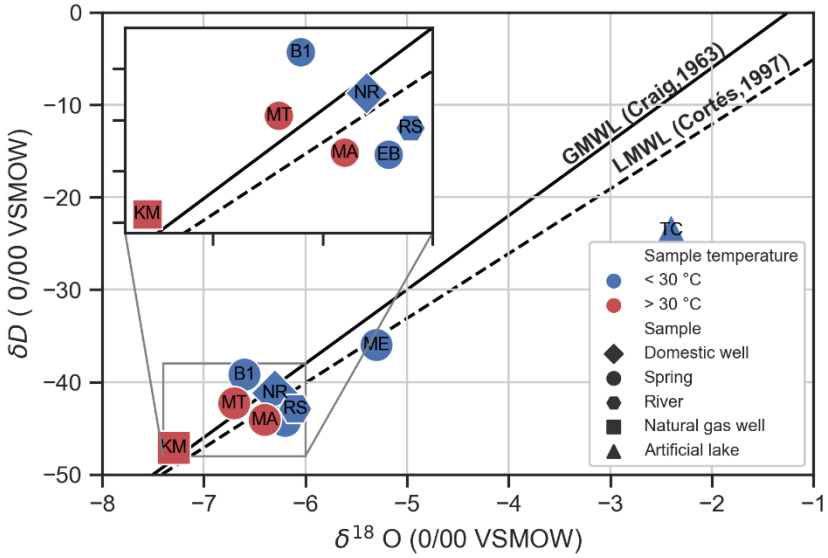

Figure 3: Plot δD vs δ 18O of the samples, including the local and global meteoric lines.

According to Güleç (2013), the extremes samples (KM and ME) could be attributed to different recharge altitudes, while the clustered groundwater samples remain as water mixed from these two extremes or show different recharge altitudes. To test this, the recharge altitude for groundwaters was estimated according to the equation proposed by Cortés & Durazo (2001).

$$\delta\,18O = -2.37Z - 3.2 \quad (1)$$

Where Z is the elevation in kilometers. The results are shown in Table 2.

Table 2: Recharge altitude for the groundwaters. Site location and elevation as reference

Site	Sample type	Latitude	Longitude	Altitude [m.a.s.l.*]	Recharge altitude [m.a.s.l*]
NR	Domestic well	27.236°	-101.222°	396	1308
B1	Spring	27.435°	-101.478°	586	1435
ME	Spring	27.28°	-101.425°	462	886
EB	Spring	27.088°	-101.557°	488	1266
MA	Spring	27.147°	-101.547°	466	1350
KM	Natural gas well	27.036°	-101.345°	484	1730
MT	Spring	27.222°	-101.233°	400	1477

*Meters above sea level

The recharge altitudes estimated for the ground waters are in the range of 886 - 1730 m.a.s.l. , being the extremes KM and ME. Comparing this range of altitudes with the local and regional relives around the study zone, it is found that the recharge altitude for sample KM and the clustered samples are located mainly outside the study zone, as the relives in those mountains range from 1300 m.a.s.l. to the 2000 m.a.s.l. ME recharge altitude is similar to the altitude of the nearest anticline and in the altitude range where the alluvial fans are located. The lithology of the mountains outside the study area and in the range of the recharge altitude corresponds to limestone and shales, lithologies associated with the formations of the regional aquifer (Cupido, Aurora), and to those of interest in natural gas (SGM, 2008).

Associating the results from this section, the waters from the first group (Ca2-HCO3) correspond to the lowest recharge altitude, probably in unconsolidated lithologies, which would explain the lowest EC values as the residence time within the lithology is short, this also explains the high levels of HCO3 in these waters. For the Ca2- SO4 groundwaters, the recharge altitude happens at higher altitudes, thus it experiences longer residence time in calcareous lithologies where the addition of SO4 ion is probably due to the dissolution of anhydrite or gypsum. As this water infiltrates deep, it is heated and then emerges and experiences a mixing process with waters from the first group, which would explain that the groundwater samples clustered in the isotope plot, between KM (highest temperature and recharge altitude) and ME (Lowest EC and lowest recharge altitude). Finally, the addition of Cl and Na in

surface waters and some springs would be explained by an evaporation process or the concentration of these kinds of minerals in lithologies that could not be identified in this work. This chemical evolution is in accordance with the evolution of waters in sedimentary basins from recharge zones to discharge zones (Tóth, 1999).

4.2 Fluid geothermometry and mixing model

To estimate pseudo-equilibrium temperatures in the thermal waters (KM, MT, MA), ten solute geothermometers were applied, the results are shown in Table 3. These temperatures were calculated using the SolGeo software, developed by Verma et al. (2008), in addition to geothermometers reported in the literature.

Table 3: Pseudo equilibrium temperatures estimated with solute geothermometers for thermal waters. Temperatures in °C

		KM	MT	MA
	Sample temperature [°C]	65.4 ± 0.1	42.4 ± 0.0	30.6 ± 0.2
Geothermometer	Reference			
TSiO20 (Silica)	Verma & Santoyo, 1997	85.6	70.8	74.5
TSiO2 (Chalcedony)	Fournier, 1977	53.8	38.4	42.1
TNa/K	Santoyo & Díaz-González, 2010	96.1	199.4	64.4
TNa-K-Ca-Mg	Fournier & Truesdell, 1973	72.8	N.A	66.9
TNa-K-Mg	Nieva & Nieva, 1987	84.8	N.A	76.2
TK-Mg	Fournier, 1991	96.6	122.6	80.9
TK-Mg	Giggenbach, 1988	18.5	14.9	21
TLi-Mg	Kharaka & Mariner, 1988	2.8	2.8	12.5
TNa-Li	Kharaka et al., 1982	104	168.3	102.4
TNa-Li	Verma & Santoyo, 1997	39.3	109.4	37.7
	Mean temperature[1]	90 ±11	134 ± 50	68 ± 21

1: Without temperatures less than the sample temperature. N.A: The sample does not meet geothermometer applicability

Most of the estimations fall below 100 °C with some exceptions, especially the Na-Li and Na/K geothermometers, where the highest temperatures are estimated. Additionally, some geothermometers (Chalcedony, Li-Mg, K-Mg, Na-Li) estimate unrealistic temperatures, as these temperatures are lower than the discharge temperature. These last estimations were not considered for the estimation of a mean reservoir temperature.

To estimate the likely reservoir water temperatures, under the premise that the thermal waters have a common source, a statistical procedure was applied. First, an analysis based on outlier detection/rejection assuming a normal distribution was applied to every site, then a two-way analysis of variance (ANOVA) was applied under the hypothesis *H0: Pseudo equilibrium temperatures estimated in one site, are statistically similar among the other sites*. If *H0* is accepted, then the estimations of the sites that are statistically similar are grouped. The statistical tests were calculated in the program UDASYS (Verma et al., 2013). For the outlier detection/rejection test, an α =0.4 was used and for the ANOVA test, it was an α =0.01.

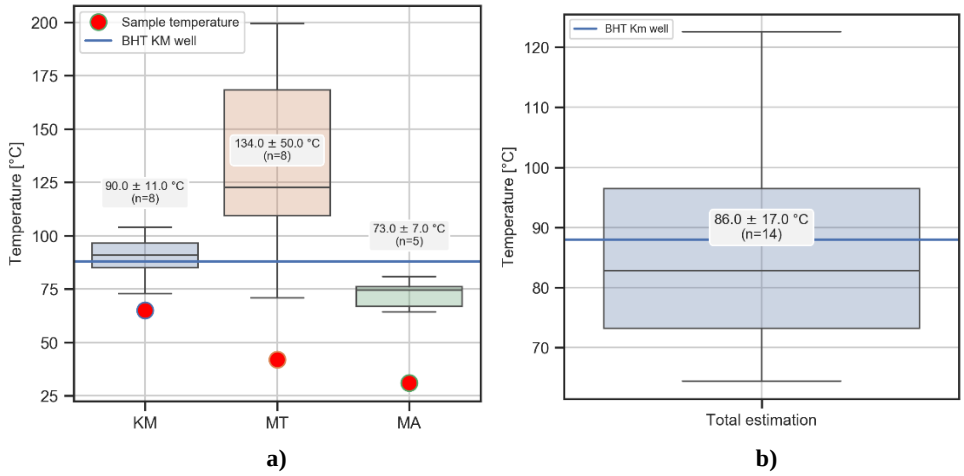

Figure 4: Boxplots of a) pseudo equilibrium temperatures after the outlier detection/rejection test in every site and b) grouped temperatures of all sites after the ANOVA and outlier detection/rejection tests. It is included the BHT of the KM well for reference.

For the first test, only in MA were identified and rejected three outliers (Both Na-Li and Chalcedony geothermometers). The boxplot diagram for the estimation per site is shown in figure **4a,** where the high, medium and low mean temperatures are MT, KM, and MA

respectively. And for the ANOVA test, no difference among the sites was found as the test F value estimated was 5.9, less than the F critic value of 6.7, thus H0 is accepted, and the temperature estimations are grouped. Additionally, an outlier detection/rejection test was applied to the grouped estimations with an α=0.01 in which the test identified as outliers and rejected the two upper temperatures (Na/K and Na-Li geothermometers in MT). After the test, the likely reservoir temperature would be 86 ± 17 °C shown in figure **4b.**

Additionally, as some degree of mixing is evidenced by the stable isotopes, a Silica-Enthalpy mixing model was constructed (Figure 5), to estimate the composition and temperature of the likely reservoir water. According to the model, the estimated source temperature or reservoir would have a temperature of 86 °C and 358.5 mg/kg of SiO2. This temperature is like the mean temperature estimated by the geothermometers after the statistical procedure, these results typify the system as low to medium temperature.

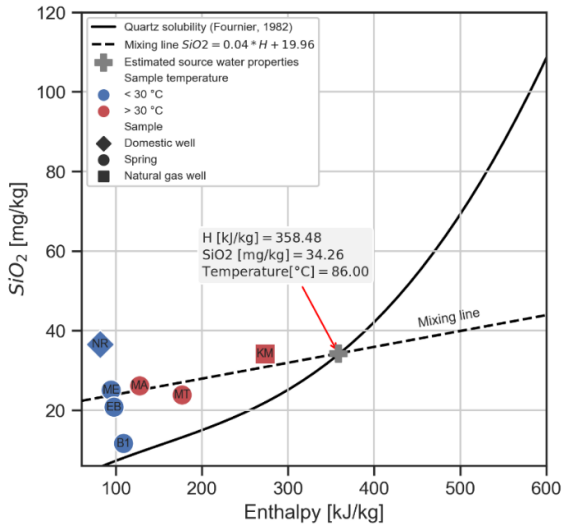

Figure 5: Silica-enthalpy mixing model for the groundwaters

4.3 Natural gas well information and deep of the reservoir

According to the information available from wells drilled within the zone (Internal reports, PEMEX), the geothermal gradient for the study zone is 29 ± 1 °C/km. This gradient is less than the normal gradient of the earth, which could show the conductive heat regime to which the fluids and the rocks at depth are exposed. With this gradient, the depth range in which the geothermometer temperatures are found would be 2600 ± 600 meters. This depth range corresponds in some wells to the Cupido formation and the La Virgen formation, this last one is the main formation objective for natural gas exploitation.

Cupido formation has a lithology of limestones while La Virgen formation is divided into three dolomitic limestone members interleaved by two evaporative (anhydrite) members that act as cap rock. Other important evidence presented during drilling at La Virgen formation is the upwelling of water and loss of drilling fluid in wells KM (Sampled) and Chicharra I (Fig. 6).

Finally, the La Virgen formation top can be found and drilled at 935 meters while the bottom at 3578 meters, this range includes the range of depth at which the geothermometers temperatures are found and at which, upwelling water was reported. To this, it is considered that the La Virgen formation is the lithology that probably hosts the thermal fluids, as the lithology of the formation can explain the addition of Ca2 and SO4 for the geochemical signature of the Ca2-SO4 thermal waters, plus the evidence of upwelling water presented during drilling at this formation.

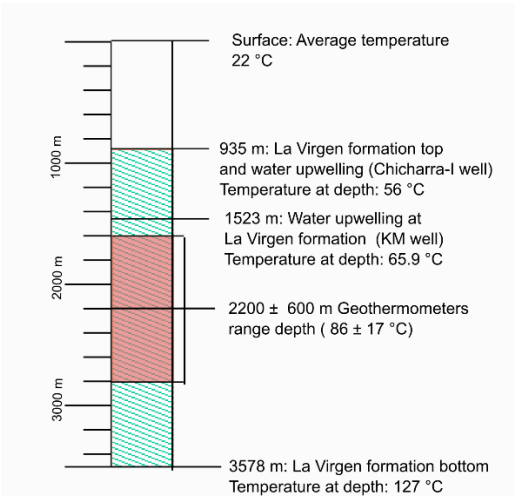

Figure 6: Evidence of temperature and upwelling water at La Virgen formation

4.4 Preliminary conceptual model for the study zone

The preliminary conceptual model, according to the information exposed before is described. The isotopic results show that the waters in the system have a meteoric origin, which precipitates at the relieves that surround the study zone. After precipitation, the fluids infiltrate through the rock and are driven and heated at depth by a conductive heat flow, in which a gravity-driven flow is also present, as the water moves from high-elevation recharge zones to the discharge zones at lower elevations. The paths that permit the ejection of the thermal fluids are associated with fractures at the base of anticlines, while the artesian flow of thermal water in some gas natural gas wells reveals the high pressure at which the probable reservoir is found.

The probable reservoir would be in La Virgen formation, as this is a formation of dolomitic limestone with some intervals of anhydrite that works as cap rock, this lithological framework justifies the addition of Ca2 and SO4 ions, which led to the formation of thermal Ca2-SO4 type waters. The probable temperatures at the reservoir would be 86 ± 17 °C according to geothermometer data, which classifies the hydrothermal system as low to medium temperature. This thermal water while ascending can be mixed with shallow Ca2-HCO3 cold waters, as isotopic data and the Silica-Enthalpy model showed.

The heat source would be identified as a normal heat flow, as the geothermal gradient within the zone is in the range of a normal gradient for the earth, furthermore, the isotopic data doesn't show isotopic firms that could be attributed to a different heat source.

4.5 Heat in rock and technical potential

With the former evidence, as the La Virgen formation is considered as the formation that host the thermal fluids, the resource assessment was estimated using the heat in place equation and a Monte Carlo simulation, as shown in the next equation

$$Q_r = Ah\rho_r Cp_r(1-\varphi)\left(T - T_{ref}\right) \quad (2)$$

Where Q_r, A, h, ρ_r, Cp_r, φ, T, T_{ref} are heat in place, area, thickness, density, specific heat capacity, porosity, temperature of the reservoir (Geothermometers) and reference temperature, respectively. For the Monte Carlo simulation, a probabilistic distribution was assigned to every variable, according to the results exposed before and from the literature. The simulation was carried out by the *NIST Uncertainty machine* (NIST, 2021) assuming a million iterations and a seed value of 95 for the random number generator.

The probabilistic functions used for the simulation are shown in table 4. The area was defined according to Iglesias & Torres (2003), minimum, medium, and max values are 1 km, 2 km, and 3 km respectively, for every thermal manifestation, in this work considered 4 thermal manifestations (Three sampled and one identified by reports of PEMEX and aerial images). Minimum, medium and max reservoir thickness was defined according to the information of gas wells within the zone (Internal report, Pemex 1981). Porosity values were reported by Eguiluz de Antuñano (2001) while density, and specific heat capacity values were estimated for La Virgen formation at an adjacent gas field by Camacho Ortegon (2009). Reference temperatures are the average minimum, medium, and max temperatures reported for the zone (CONAGUA, 2021).

Table 4: Probabilistic distributions of the variables used in the Monte Carlo simulation

Triangular distributions	Min value	Med value	Max value
Area (A) [km^2]	4	8	12
Thickness (h) [m]	223	766	1190
Reference temperature (T_{ref}) [°C]	7.7	22	33.9
Porosity (φ) *	0.06		0.08
Gaussian distributions	**Mean**		**Std deviation**
Geothermometer temperatures (T) [°C]	86.1		17.4
Density (ρ_r) [kg/m^3]	2649.5		11.2
Heat capacity (Cp_r) [$kJ/kg°C$]	0.951		0.005

*Symmetric triangular distribution

The results and statistical parameters from the simulation are shown in table 5. The mean value for the heat in rock is 883 ± 402 PJ. For the other parameters, the values seem to be seized to the left, as the thickness values and other variables show a predominance of values to the left. The mean value would represent 5.5 % of the heat in place of the state of Coahuila, according to the work of Iglesias & Torres (2003) which is 15.27 EJ, calculated for 17 thermal manifestations and 12 geothermal systems. Additionally, with the results of the simulation, a technical potential can be calculated by dividing the heat in place by an average utilizing time and then applying a recovery factor to the heat (Limberger et al., 2018). The calculation considered an average time of 30 years and a recovery factor of 2%, a minimal value for enhanced systems (Grant, 2014). Thus, an average rounded technical potential of 19 ± 8 MWt and an average value per manifestation of 4.425 MWt is estimated for the study zone.

Table 5: Statistical parameters for the Heat in place and technical potential in the study zone. Limits at α = 0.05

Statistical parameter	Heat in place [PJ]	Technical potential [MWt]
Media	883	18.7
Std deviation	402	8.5
Median	827	17.5
Mode	390	8.2
Lower limit	270	5.7
Upper limit	1820	38.5

5. CONCLUSIONS

Thermal manifestations and cold waters within the study area of Escobedo were studied and analyzed. It was found that waters within the study zone have a meteoric origin, in which recharge occurs at elevations that surround the study area, with two different geochemical features related to the recharge elevation and lithological setting. Ca2-HCO3 waters were identified in some samples, associated with the water of recent recharge at unconsolidated lithologies (Alluvium or conglomerates), so low presence of ions, while Ca2-SO4 waters were identified in thermal samples, which precipitation occurs in calcareous lithologies at a high elevation far away from the discharges zone, that leads to higher residence times within the rock. It was found that the thermal waters experience some degree of mixing with cold waters, as isotopic data and the Silica-enthalpy mixing model showed.

The thermal fluids preset pseudo equilibrium temperatures of 86 ± 17 °C, a temperature range in agreement with the silica-enthalpy model. These temperatures permit classify the geothermal resource as low to medium temperature. The thermal gradient within the zone suggests that these temperatures could be found at La Virgen formation, formation of dolomitic limestone with anhydrite members, which also explains and justify the addition of Ca2 and SO4 ions, geochemical signatures of thermal water. Additionally, data from natural gas wells shows that the temperatures found at this formation and the events of upwelling water during drilling permitted identified La Virgen formation as the reservoir formation.

The resource assessment for the zone shows that the resource presents a heat in place of 883 ± 402 PJ, while the technical potential presents values of 19 ± 8 MWt. Nevertheless, additional studies, including geochemical and geophysical, and detailed study of gas well data are required to refine the estimations of the resource. Finally, at the study zone, the information from gas well data can contribute to the subsequent phases of exploration or exploitation of the resource.

REFERENCES

Camacho Ortegon, L. F.: Origine-Evolution-Migration et Stockage, des hydrocarbures dans le bassin de Sabinas, NE Mexique: étude intégré de pétrographie, géochimie, géophysique et modélisation numérique 1D-2D et 3D, (PhD's thesis) Université de Lorraine, (2009).

CONAGUA.: Información Estadística Climatológica, Retrieved August 17, 2021, from https://smn.conagua.gob.mx/es/climatologia/informacion-climatologica/informacion-estadistica-climatologica

Corona-Esquivel, R., Tritlla, J., & Benavides-Muñoz, M. E.: Geología , estructura y composición de los principales yacimientos de carbón mineral en México, *Boletín de La Sociedad Geológica Mexicana*, **57**, (2006), 141–160.

Cortés, A., & Durazo, J.: Tendencia del oxígeno-18 en la precipitación del centro de México, *Ingenieria Hidraulica En Mexico*, **16**(2), (2001) 93–102.

Cortés, A., Durazo, J., & Farvolden, R. N.: Studies of isotopic hydrology of the basin of Mexico and vicinity: annotated bibliography and interpretation, *Journal of Hydrology*, **198**(1–4), (1997), 346–376. https://doi.org/10.1016/S0022-1694(96)03273-8

Craig, H.: Isotopic Variations in Meteoric Waters, *Science*, **133**(3465), (1961), 1702–1703. https://doi.org/10.1126/science.133.3465.1702

Cuevas Leree, J. A.: Analysis of subsidence and thermal history in the Sabinas Basin, northeasern Mexico, (PhD's thesis) University of Arizona, (1984).

Eguiluz de Antuñano, S.: Geologic Evolution and Gas Resources o f the Sabinas Basin in Northeastern Mexico. In C. Bartolini, R. T. Buffler, & A. Cantú-Chapa (Eds.), *The Western Gulf of Mexico Basin: Tectonics, Sedimentary Basins, and Petroleum Systems*, (2001) (pp. 241–270). Ameican Association of Petroleum Geologists.

Fournier, R. O., & Truesdell, A. H.: An empirical Na-K-Ca geothermometer for natural waters, *Geochimica et Cosmochimica Acta*, **37**, (1973), 1255–1275.

Fournier, R.O.: Chemical geothermometers and mixing models for geothermal systems, *Geothermics*, **5**(1–4), (1977), 41–50. https://doi.org/10.1016/0375-6505(77)90007-4

Fournier, R. 0, & Potter, R. W.: A revised and expanded silica (quartz) geothermometer. *Geothermal Resources Council Bulletin*, **11**(10), (1982) 3–12. https://doi.org/5703508

Fournier, R. O.: Water geothermometers applied to geothermal energy, In F. D'Amore (Ed.), *Applications of Geochemistry in*

Geothermal Reservoir Development, (1991), (pp. 37–69). Rome, Italy: UNITAR/UNDP Centre on Small Energy Resources.

Giggenbach, W. F.: Geothermal solute equilibria. Derivation of Na-K-Mg-Ca geoindicators. *Geochimica et Cosmochimica Acta*, **52**(12), (1988), 2749–2765. https://doi.org/10.1016/0016-7037(88)90143-3

Grant, M. A.: Stored-heat assessments: a review in the light of field experience, *Geothermal Energy Science*, **2**(1), (2014) 49–54. https://doi.org/10.5194/gtes-2-49-2014

Güleç, N.: Isotope and gas geochemistry of geothermal systems. *IGA acdemy report*, (2013)

Iglesias, E. R., & Torres, R. J.: First assessment of Mexican low- to medium-temperature geothermal reserves, *Energy Sources*, **25**(2), (2003), 161–173. https://doi.org/10.1080/00908310303433

Kharaka, Y. K., Lico, M. S., & Law, L. M. X.: Chemical Geothermometers Applied to Formation Waters, Gulf of Mexico and California Basins, *AAPG Bulletin*, **66**, (1982). https://doi.org/10.1306/03B59EAE-16D1-11D7-8645000102C1865D

Kharaka, Y. K., & Mariner, R. H.: Chemical Geothermometers and Their Application to Formation Waters from Sedimentary Basins, In *Thermal History of Sedimentary Basins*, (1989), (pp. 99–117). https://doi.org/10.1007/978-1-4612-3492-0_6

Limberger, J., Boxem, T., Pluymaekers, M., Bruhn, D., Manzella, A., Calcagno, P., … van Wees, J.-D. D.: Geothermal energy in deep aquifers: A global assessment of the resource base for direct heat utilization, *Renewable and Sustainable Energy Reviews*, **82**, (2018), 961–975. https://doi.org/10.1016/j.rser.2017.09.084

Molina, J. L., Vázquez Limón, R., & Ojeda García, A. C.: Informe Geológico-Minero Carta Primero de Mayo G14-A43 Escala 1:50000, Consejo de Recursos Minerales, (2004).

Nieva, D., & Nieva, R.: Developments in geothermal energy in Mexico-Part twelve. A cationic geothermometer for prospecting of geothermal resources, *Heat Recovery Systems & CHP*, **7**(3), (1987), 243–258.

NIST.: *NIST Uncertainty Machine*, National Institute of Standards and Technology, (2021).

Padilla Y Sanchez, R. J.: Post-Paleozoic tectonics of northeast Mexico and its role in the evolution of the Gulf of Mexico. *Geofisica Internacional*, **25**(1), (1986), 157–206.

PEMEX.: Internal report, (1981).

Santoyo, E., & Díaz-González, L.: A New Improved Proposal of the Na / K Geothermometer to Estimate Deep Equilibrium, *Proceedings*, World Geothermal Congress, 25–29, Bali, Indonesia (2010).

SGM.: Carta geológico-minera G14-1 Nueva Rosita, Coahuila y Nuevo León. Pachuca, Hidalgo: Servicio Geológico Mexicano, Secretaría de Economía, (2008).

Tester, J., Reber, T., Beckers, K., Lukawski, M., Camp, E., Aguirre, G. A., … Horowitz, F.: Integrating Geothermal Energy Use into Re-building American Infrastructure, *Proceedings*, World Geothermal Congress, 19–25, Melbourne, Australia, (2015).

Tóth, J.: Groundwater as a geologic agent: An overview of the causes, processes, and manifestations, *Hydrogeology Journal*, **7**(1), (1999), 1–14. https://doi.org/10.1007/s100400050176

Verma, S. P., Pandarinath, K., & Santoyo, E.: SolGeo: A new computer program for solute geothermometers and its application to Mexican geothermal fields, *Geothermics*, **37**, (2008), 597-621. https://doi.org/10.1016/j.geothermics.2008.07.004

Verma, S. P., & Santoyo, E.: New improved equations for Na/K, Na/Li and SiO, geothermometers by outlier detection and rejection, *Journal of Volcanology and Geothermal Research*, **79**, (1997), 9–23.

Verma, S. P., Cruz-Huicochea, R., & Díaz-González, L.: Univariate data analysis system: Deciphering mean compositions of island and continental arc magmas, and influence of the underlying crust, *International Geology Review*, **55**(15), (2013), 1922–1940. https://doi.org/10.1080/00206814.2013.810363

Wolaver, B. D., Crossey, L. J., Karlstrom, K. E., Banner, J. L., Cardenas, M. B., Gutiérrez Ojeda, C., … Sharp, J. M., Identifying origins of and pathways for spring waters in a semiarid basin using He, Sr, and C isotopes: Cuatrocienegas Basin, Mexico, *Geosphere*, 9(1), (2013), 113–125. https://doi.org/10.1130/GES00849.1